Supplementary Material

Haloturbation in the northern Atacama Desert revealed by a hidden subsurface network of calcium sulphate wedges

Aline Zinelabedin[1,2], Joel Mohren[1,3], Maria Wierzbicka-Wieczorek[1], Tibor J. Dunai[1], Stefan Heinze[4] Benedikt Ritter[1]

[1]Institute of Geology and Mineralogy, University of Cologne, Zülpicher Str. 49b, 50674 Cologne, Germany
[2]Institute of Geography, University of Cologne, Zülpicher Str. 45, 50674 Cologne, Germany
[3]Department of Geography, RWTH Aachen University, Wüllnerstr. 5b, 52062 Aachen, Germany
[4]Institute for Nuclear Physics, University of Cologne, Zülpicher Str. 77, 50937 Cologne, Germany
Correspondence to: Aline Zinelabedin (aline.zinelabedin@uni-koeln.de)

1 Outcrop and shattered clast data

Figure S.1: Close-up of trench wall showing main characteristic features of the outcrop.

Figure S.2: Desert pavement on the outcrop surface at the Aroma fan site.

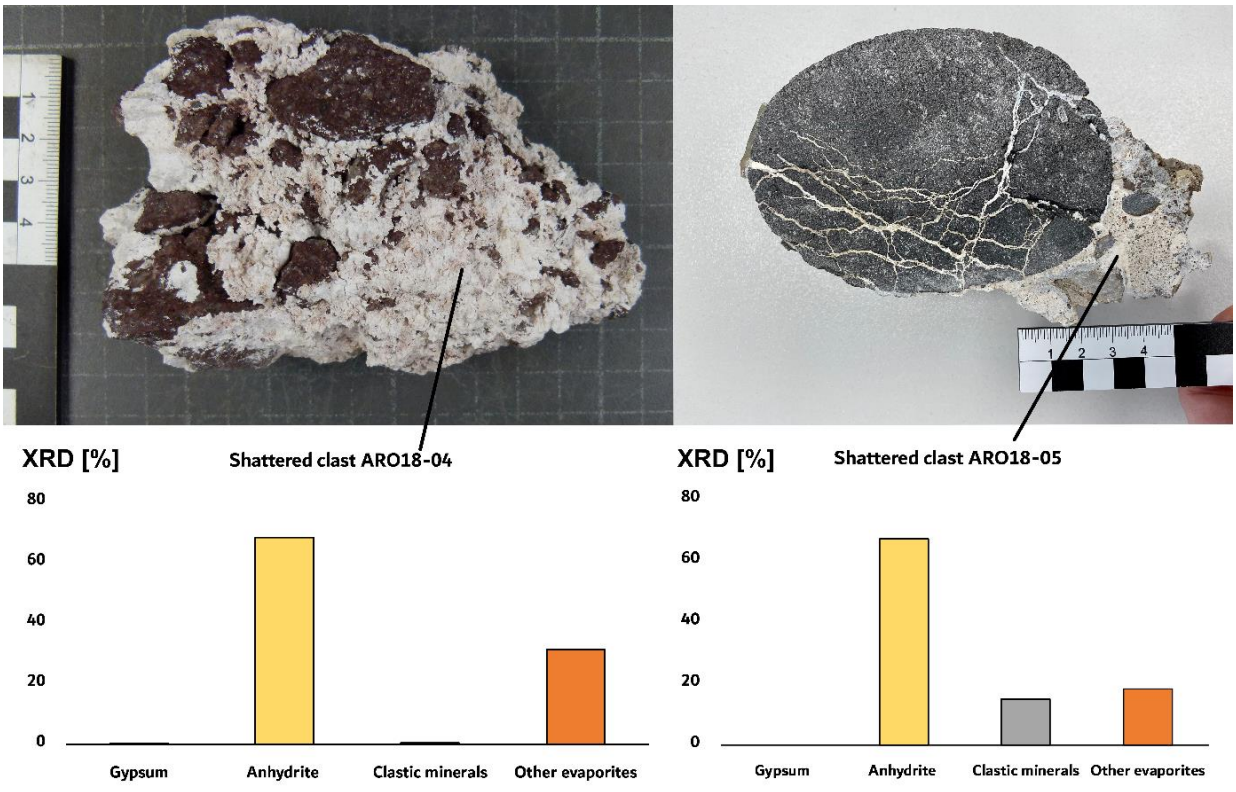

Figure S.3: Shattered clasts with calcium sulphate filling from the polygon body.

2 ^{21}Ne data

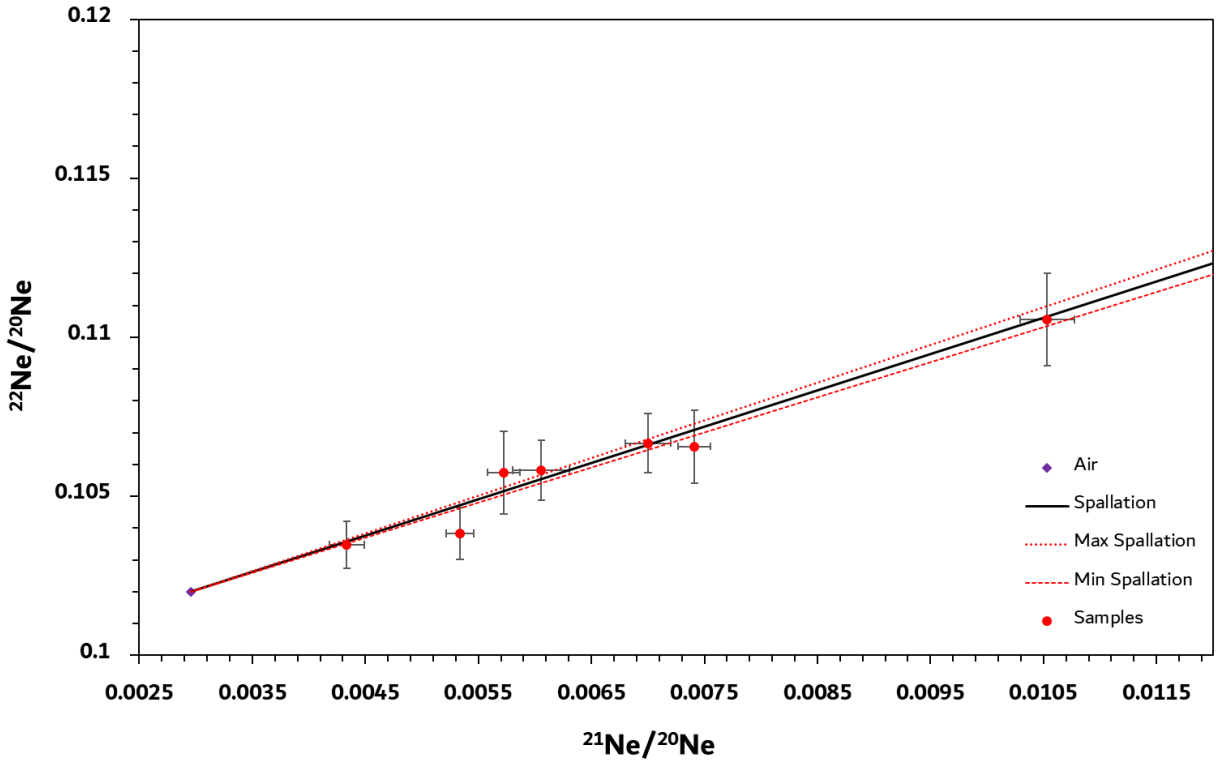

Figure S.4: Neon triple isotope diagram. The black points are the six analysed surface quartz clasts ARO17-01A–F including the CREU1 standard (Vermeesch et al., 2015). The red and black spallogenic lines represent the mixture of air and the spallogenic end member. Error bars are 1 σ.

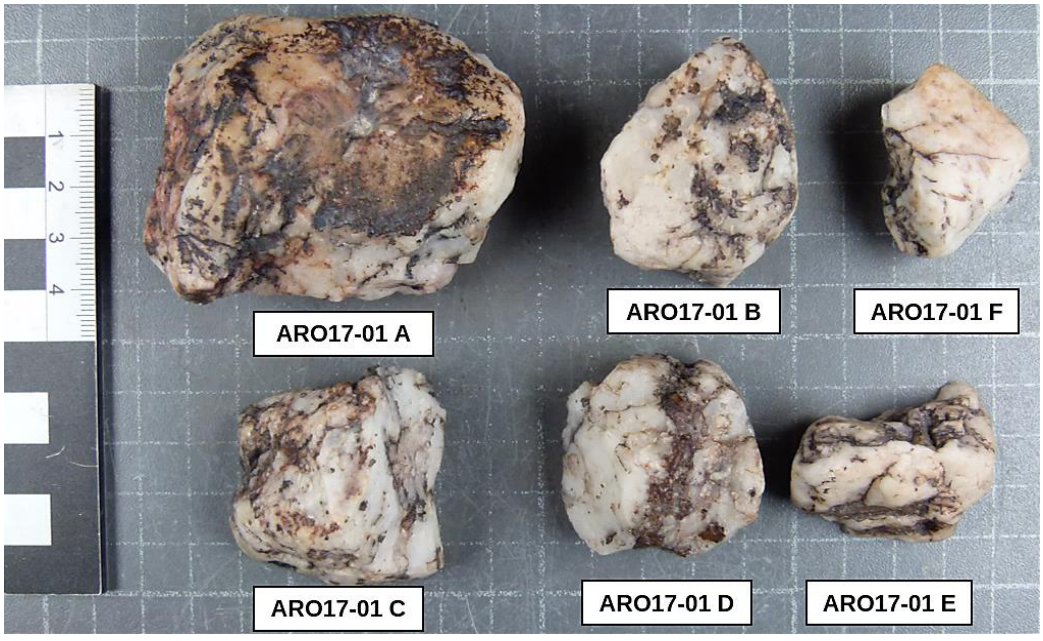

Figure S.5: Six surface quartz clasts for ^{21}Ne exposure dating from the surface nearby the Aroma fan outcrop.

Table S.1: Neon-isotope ratios of surface clasts and standard data for the neon triple isotope diagram.

Sample ID	Cologne Noble Gas ID	20Ne	d 20Ne	22/20	d 22/20	d 22/20 %	21CDD /20	d 21CDD/20	d 21/20 %	21Ne ex atoms/gr		
		atoms/g	atoms/g	Measured	Measured	d%	Measured	Measured	d%	atoms/gr	d	d%
CREU1	CGN0050	44803661018	718477516.3	0.110555846	0.001448521	1.3%	0.010533	0.000240	2.3%	$3.39x10^8$	$9.91x10^6$	2.9%
ARO17-01A	CGN0065	41081406779	726014584.8	0.106563781	0.001147927	1.1%	0.007412	0.000143	1.9%	$1.83x10^8$	$4.87x10^6$	2.7%
ARO17-01B	CGN0066	74909489207	1576581969	0.103830648	0.000816008	0.8%	0.005336	0.000125	2.3%	$1.78x10^8$	$5.67x10^6$	3.2%
ARO17-01C	CGN0067	58621031889	2353982981	0.10581425	0.000940202	0.9%	0.006056	0.000249	4.1%	$1.82x10^8$	$1.05x10^7$	5.8%
ARO17-01D	CGN0068	54288772805	1530907210	0.106670913	0.000933514	0.9%	0.007001	0.000204	2.9%	$2.19x10^8$	$8.96x10^6$	4.1%
ARO17-01E	CGN0069	60793967653	1518185161	0.105749455	0.001302841	1.2%	0.005725	0.000145	2.5%	$1.68x10^8$	$6.04x10^6$	3.6%
ARO17-01F	CGN0070	96218172047	3213967854	0.103473064	0.000745307	0.7%	0.004335505	0.000152137	3.5%	$1.33x10^8$	$6.45x10^6$	4.9%

Table S.2: Calculated ^{21}Ne exposure ages of the surface quartz clasts ARO17-01A–F from the CRONUS-Earth online calculator (Balco et al., 2008) for exposure ages based on scaling scheme LSD_n (Lifton et al., 2014) and calculation parameters.

Sample ID	Calculation parameters						Scaling LSD_n Lifton et al. (2014)		Scaling Stone (2000)		Deviation between LSD_n and Stone scaling
	Coordinates	Elevation [m a.s.l.]	Erosion rate (cm/a)	Shielding factor	Clast thickness [cm]	Sample density [g/cm³]	Age [Ma]	External error [Ma]	Age [Ma]	External error [Ma]	[%]
ARO17-01A	19°39'34''S, 69°35'51''W	1627	0 (unknown)	1	3	2.65	4.51	0.37	5.61	0.46	24.37
ARO17-01B	19°39'34''S, 69°35'51''W	1627	0 (unknown)	1	2.6	2.65	4.36	0.36	5.43	0.45	24.2
ARO17-01C	19°39'34''S, 69°35'51''W	1627	0 (unknown)	1	2.8	2.65	4.51	0.37	5.61	0.46	24.37
ARO17-01D	19°39'34''S, 69°35'51''W	1627	0 (unknown)	1	1.4	2.65	5.36	0.44	6.63	0.54	23.71
ARO17-01E	19°39'34''S, 69°35'51''W	1627	0 (unknown)	1	1.6	2.65	3.4	0.32	4.99	0.41	24.92
ARO17-01F	19°39'34''S, 69°35'51''W	1627	0 (unknown)	1	1.6	2.65	3.27	0.29	4.13	0.36	25.97
Mean							**4.34**	**0.36**	**5.40**	**0.45**	**24.64**

3 ICP-OES data

Table S.3: ICP-OES element concentration in mol/l.

ICP Sample ID	Dilution factor	Cl-line 134.724	Na-line 589.592
Surface crust			
ARO18-02-001	100	0	0
ARO18-02-002	100	0	0
ARO18-02-002A	100	0	0
ARO18-02-003A	100	0	0
ARO18-02-004	100	0	0
ARO18-02-005	100	0	0
ARO18-02-006	100	0	0
ARO18-02-007	100	0	0.77
Shattered clasts			
ARO18-02-04	100	0	0
ARO18-02-05	100	0.68	1.46
Subsurface wedge			
ARO18-08-LP1	100	0	0.97
ARO18-08-LP2	100	0	1.07
ARO18-08-LP3	100	0	1.13
ARO18-08-LP4	100	0.44	1.31
ARO18-08-LP5	100	0.36	1.21
ARO18-08-LP6	100	0.50	1.40
ARO18-08-LP7	100	0.75	1.71
ARO18-08-LP8	100	0.34	1.32
ARO18-08-LP9	100	0.34	1.35
ARO18-08-LP10	100	0.42	1.44
ARO18-08-RP1	100	0	1.15
ARO18-08-RP2	100	0	1.32
ARO18-08-RP3	100	0	0.95
ARO18-08-RP4	100	0	0.96
ARO18-08-RP5	100	0.60	1.17
ARO18-08-RP6	100	0.70	1.09
ARO18-08-RP7	100	0	0
ARO18-08-RP8	100	0	0
ARO18-08-RP9	100	0	0
ARO18-08-RP10	100	0	0

4 XRD data

Table S.4: XRD results (individual phases) of wedge, crust, and shattered clast subsamples.

Sample	Goodness of fit (GOF) value	Gypsum	Anhydrite	Aluminite	Konyaite	Halite	Quartz	Albite	Anorthite	Hornblende	Pargasite	Muscovite	Dolomite	Arcanite	Othoclase	Fluoro-riebeckite	Amarantite	Labradorite	Peretaite	Ramsbeckite	Alunogen
Surface crust																					
ARO18-02-001	2.16	0.78	-	35.41	-	-	7.42	12.02	6.34	10.09	-	8.17	-	-	6.88	-	-	0.42	-	8.05	4.43
ARO18-02-002	2.06	87.81	0.52	0.96	-	-	4.53	6.17	-	-	-	-	-	-	-	-	-	-	-	-	-
ARO18-02-002A	2.21	91.9	1.04	0.49	-	-	2.86	3.7	-	-	-	-	-	-	-	-	-	-	-	-	-
ARO18-02-003A	2.04	92.24	1.72	-	1.52	-	2.55	1.97	-	-	-	-	-	-	-	-	-	-	-	-	-
ARO18-02-004A	2.18	87.06	1.76	-	-	-	7.84	3.34	-	-	-	-	-	-	-	-	-	-	-	-	-
ARO18-02-005	1.85	94.84	2.17	-	-	-	2.13	0.86	-	-	-	-	-	-	-	-	-	-	-	-	-
ARO18-02-006	2.10	91.4	3.53	-	-	-	2.44	2.63	-	-	-	-	-	-	-	-	-	-	-	-	-
ARO18-02-007	1.91	72.6	23.93	-	1.21	-	1.83	0.43	-	-	-	-	-	-	-	-	-	-	-	-	-
Subsurface wedge																					
ARO18-08-RP1	2.20	0.6	62.72	3.17	-	-	5.26	16.74	-	-	1.55	9.56	-	-	-	-	0.41	-	-	-	-
ARO18-08-RP2	2.12	0.9	41.6	0.77	-	-	9.41	40.78	-	-	2.88	3.66	-	-	-	-	-	-	-	-	-
ARO18-08-RP3	2.58	0.42	51.25	-	-	-	9.06	33.22	2.83	-	1.02	2.19	-	-	-	-	-	-	-	-	-
ARO18-08-RP4	2.40	2.87	40.02	-	-	-	7.83	29.19	15.67	-	3.05	1.58	-	-	-	-	-	-	-	-	-
ARO18-08-RP5	2.13	0.05	46.4	4.44	-	-	7.17	28.8	-	-	0.07	13.06	-	-	-	-	-	-	-	-	-
ARO18-08-RP6	2.34	0.31	53.64	-	-	-	8.42	17.61	0.31	-	0.32	1.71	-	-	5.97	0.21	-	11.51	-	-	-
ARO18-08-RP7	2.43	0.28	53.14	-	-	-	3.69	35.99	-	-	0	6.82	-	-	-	-	-	-	0.06	-	-
ARO18-08-RP8	2.42	16.69	32.8	-	-	-	6.69	28.5	8.76	-	1.01	0.84	-	-	4.64	0.07	-	-	-	-	-
ARO18-08-RP9	2.99	40.59	3.04	0.8	-	-	5.51	22.64	15.69	-	5.55	3.13	-	-	2.44	0.57	-	-	-	-	-
ARO18-08-RP10	2.99	39.8	2.98	0.76	-	-	5.68	24.29	15.46	-	5.6	3.13	-	-	1.74	0.55	-	-	-	-	-
ARO18-08-LP1	2.19	-	49.75	0.06	-	-	5.56	34.75	0.2	0.89	0.04	8.77	-	-	-	-	-	-	-	-	-
ARO18-08-LP2	1.96	-	65.59		-	-	7.28	23.58	0.28	1.62	-	-	0.36	1.3	-	-	-	-	-	-	-
ARO18-08-LP3	2.04	-	68.04	2.8	-	-	6.05	5.28	12.05	1.64	-	4.14	-	-	-	-	-	-	-	-	-
ARO18-08-LP4	2.18	-	73.49	-	-	-	3.62	18.48	0.38	0.42	-	-	-	0.1	-	-	-	-	-	-	-

ARO18-08-LP5	2.54	-	49.33	0.7	-	-	8.56	8.52	17.17	-	-	-	-	-	15.73	-	-	-	-	-	-
ARO18-08-LP6	2.06	-	53.61	1.66	-	-	9.06	32.5	0.19	-	-	-	-	-	-	2.98	-	-	-	-	-
ARO18-08-LP7	2.24	-	71.56	1.92	-	-	8.95	17.55	0.02	-	-	-	-	-	-	-	-	-	-	-	-
ARO18-08-LP8	2.03	-	50.07	1.02	-	-	10.25	37.45	-	1.23	-	-	-	-	-	-	-	-	-	-	-
ARO18-08-LP9	2.09	-	58.88	0.35	-	-	8.77	31.67	-	0.32	-	-	-	-	-	-	-	-	-	-	-
ARO18-08-LP10	2.35	-	68.9	1.18	-	-	5.66	19.45	-	0.63	-	-	-	-	4.18	-	-	-	-	-	-
Shattered clasts																					
ARO18-04	2.17	0.09	68.23	30.39	0.81	-	-	0.48	-	-	-	-	-	-	-	-	-	-	-	-	-
ARO18-05	2.62	-	67.11	17.6	-	0.54	9.4	5.36	-	-	-	-	-	-	-	-	-	-	-	-	-

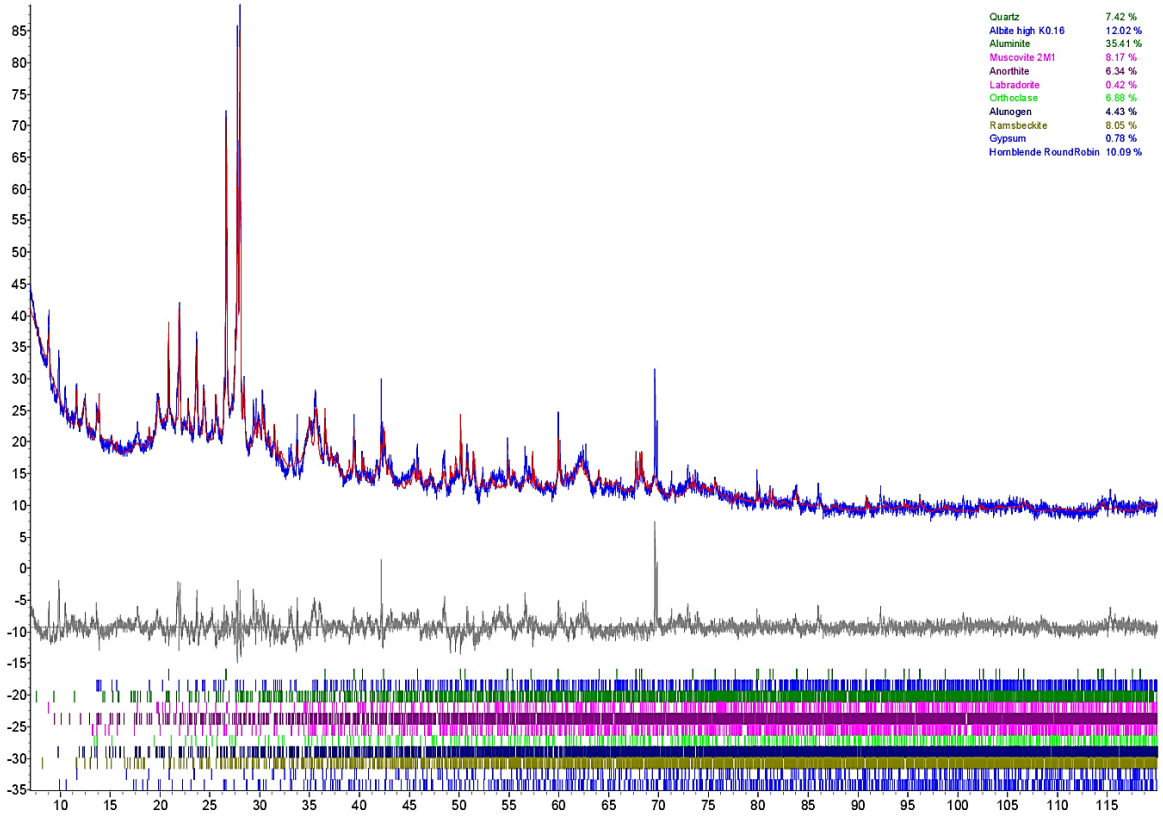

Figure S.6: XRD diffractogram of surface subsample ARO18-02-001 showing a high amount of aluminite.

5 Plutonium data

Table S.5: ^{239}Pu data of surface crust subsamples.

Sample ID[a]	Depth b.s.	Batch ID	Mass	Carrier mass			^{239}Pu/^{242}Pu			Blank subtraction	^{239}Pu specific activity		
	(cm)[b]		(g)	(g)[c]			(x10^{-3})[d]			^{239}Pu (%)	(mBq kg^{-1})[e]		
ARO18-02-001	0	Col22-1	20.49	0.2291	±	0.0001	11.75	±	0.35	1.7	6.48	±	0.20
ARO18-02-TC2	0	Col23-3	20.73	0.2302	±	0.0001	11.66	±	0.41	6.2	6.09	±	0.23
ARO18-02/Pu2	0-1.5	Col22-1	11.57	0.2301	±	0.0001	0.61	±	0.07	32.8	0.41	±	0.08
ARO18-02/Pu3	1.5-3	Col23-2	9.22	0.2308	±	0.0001	1.32	±	0.10	52.5	0.78	±	0.16
ARO18-02/Pu4	3-4.5	Col22-1	7.46	0.2306	±	0.0001	0.97	±	0.09	20.5	1.19	±	0.15
ARO18-02/Pu5	~10	Col22-1	4.25	0.2301	±	0.0001	3.40	±	0.21	5.9	8.68	±	0.59

[a] All samples taken at 19° 39'34.02''S, 69° 35' 51.4''W

[b] Depth below the top crust surface

[c] ^{242}Pu carrier solution concentration 22.13 ppt

[d] Ratios measured by CologneAMS with 1σ measurement uncertainties

[e] After blank correction with propagated 1σ uncertainties

Table S.6: ^{240}Pu data of surface crust subsample ARO18-02-TC2.

Sample ID	Depth b.s.	Batch ID	Mass	Carrier mass			^{240}Pu/^{242}Pu			Blank subtraction	^{240}Pu specific activity			^{240}Pu/^{239}Pu		
	(cm)[a]		(g)	(g)[b]			(x10^{-3})[c]			^{240}Pu (%)	(mBq kg^{-1})[d]			(x10^{-3})[d,e]		
ARO18-02-TC2	0	Col23-3	20.73	0.2302	±	0.0001	2.59	±	0.19	22.1	4.13	±	0.41	0.185	±	0.020

[a] Depth below crust surface

[b] ^{242}Pu carrier solution concentration 22.13 ppt

[c] Ratios measured by CologneAMS with 1σ uncertainties

[d] After blank correction with propagated 1σ uncertainties

[e] See main manuscript for ^{239}Pu data

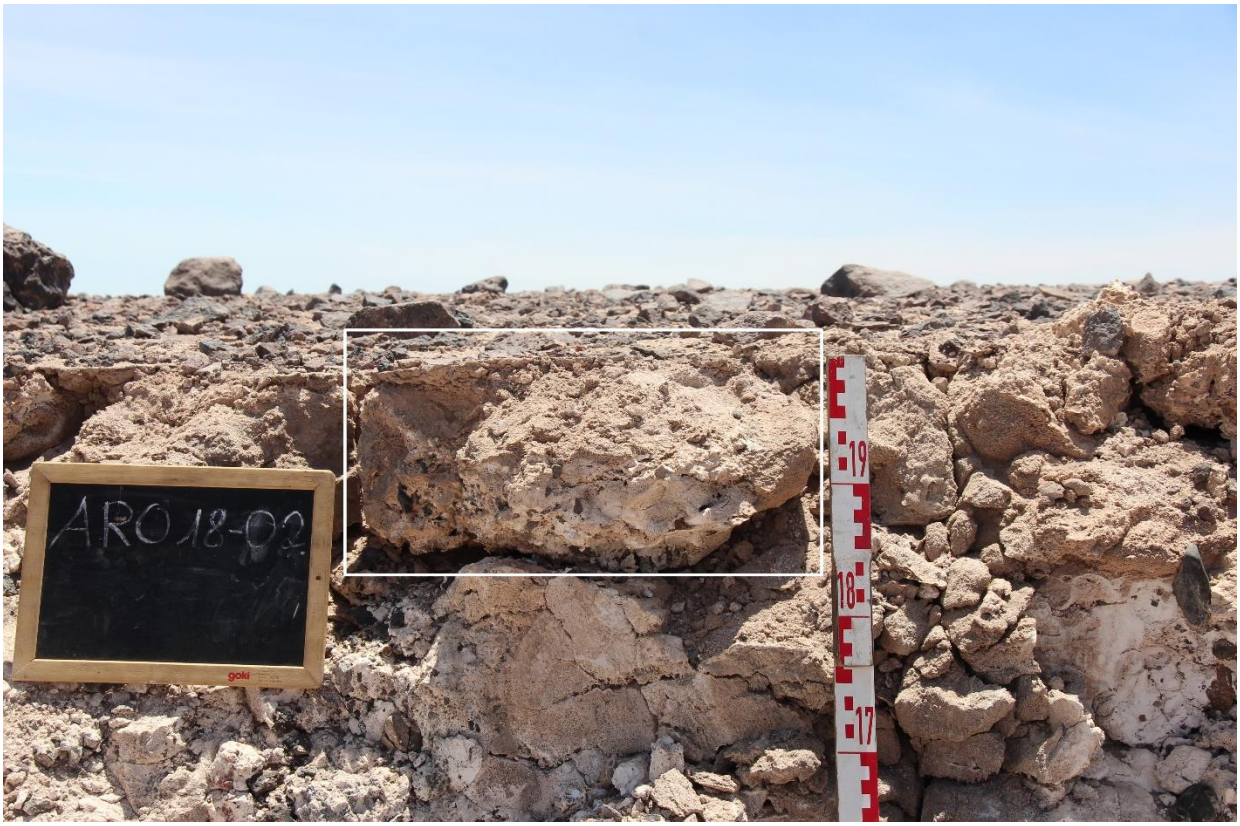

Figure S.7: Position of surface-crust sample in the outcrop (white box). Surface-crust subsample ARO18-02 is a crust block taken as a part of this pristine surface-crust sample marked with the white box.

Figure S.8: Two photos of surface-crust subsample block ARO18-02 and markers of Pu subsamples positions of subsamples ARO18-02/Pu2, 3, 4. Samples ARO18-02-001 and the replicate sample ARO18-02-TC2 were taken from the top surface of the crust block.

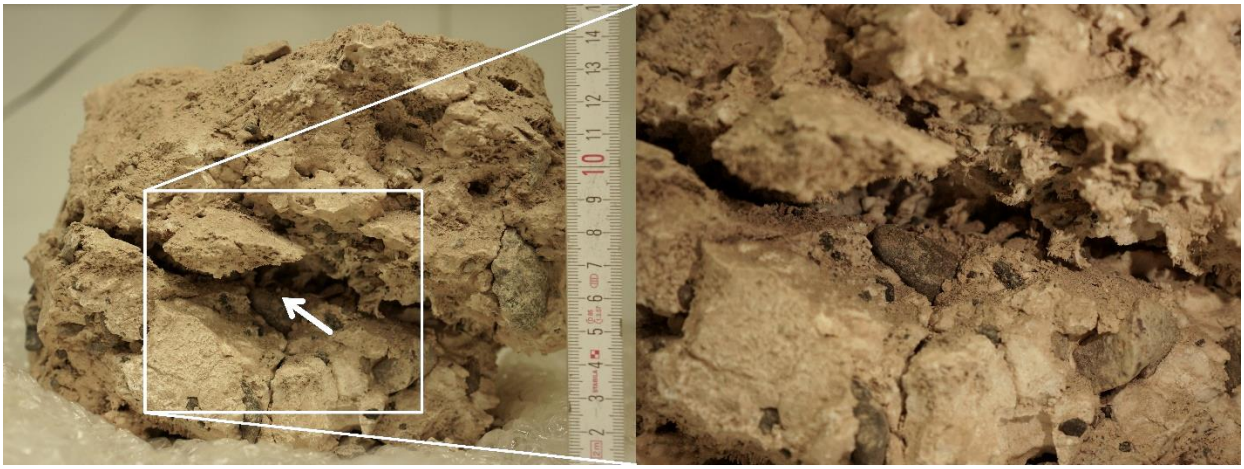

Figure S.9: Left: Photo of crust crack where the Pu subsample ARO18-02/Pu5 was subsampled. Right: close-up of the crack.

6 Sample pucks for SEM analysis

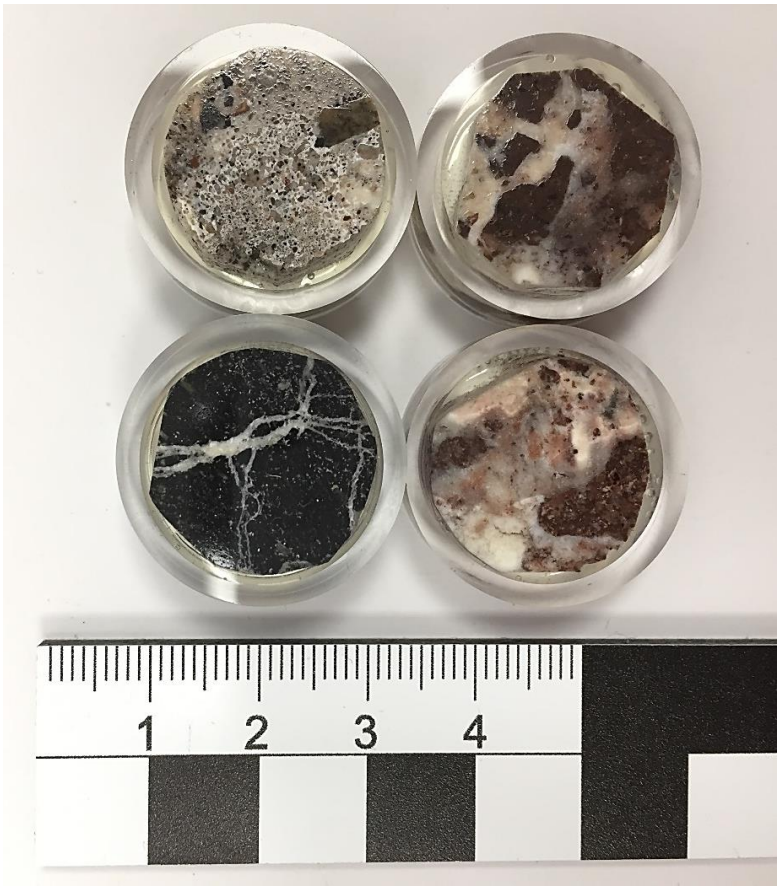

Figure S.10: Sample pucks of shattered clast samples (with salt filling) for SEM imagery. All samples are embedded in epoxy resin.

7 Photogrammetry

Methodology

For a comprehensive description of digitalising objects using a lightbox setup see e. g. Leménager et al. (2023). The camera (Sony Alpha NEX-7, 24.3 mega pixels) was mounted on a tripod and images were taken at a distance of ~ 30 cm (ARO17-03A) and ~ 45 cm (ARO18-02) between the camera lens (Sony SEL35F18, 54 mm full format equivalent f/1.8 fixed-focal-length lens) and the specimen. During each run, the turntable horizontally rotated the specimen by 360 degrees. During image acquisition of sample ARO17-03A, four scale bars were photographed together with the specimen. The sample was turned upside down and pictured in four runs (~40 pictures per run, camera tilted by ~45°) to ensure sufficient image coverage per specimen surface area (for basic principles of structure for motion multiview stereopsis (SfM-MVS) photogrammetry method see e. g. Luhmann et al. 2010). The more fragile crust block sample ARO18-02 could not be turned upside down and was thus photographed from two different camera positions (~45° and ~10°

camera tilt) with a total picture count of 97. Scaling of the 3D model was achieved by measuring the spatial distances between five distinct features appearing on the crust's surface using a calliper. The image datasets were subsequently processed using Agisoft Metashape Professional Software (ver. 1.7.5). The reconstruction quality was improved by adopting the point cloud optimisation procedures suggested by Over et al. (2021).

Table S.7: Photogrammetry data of surface crust and wedge sample.

Sample ID	Mass (g)			Volume (cm^3)[a]			Density ($g\ cm^{-3}$)		
ARO17-03A	278.74	±	0.01	166.02	±	3.87	1.68	±	0.04
ARO18-02	4031.0	±	0.5	3014.29	±	70.24	1.34	±	0.03
[a] Volume uncertainties empirically derived (cf. Mohren et al. 2020b). [b]Lower level of precision ignored in calculations (cf. Mohren et al, 2020b)									

ColSfM4-ARO17-03A

Processing Report

18 May 2023

Survey Data

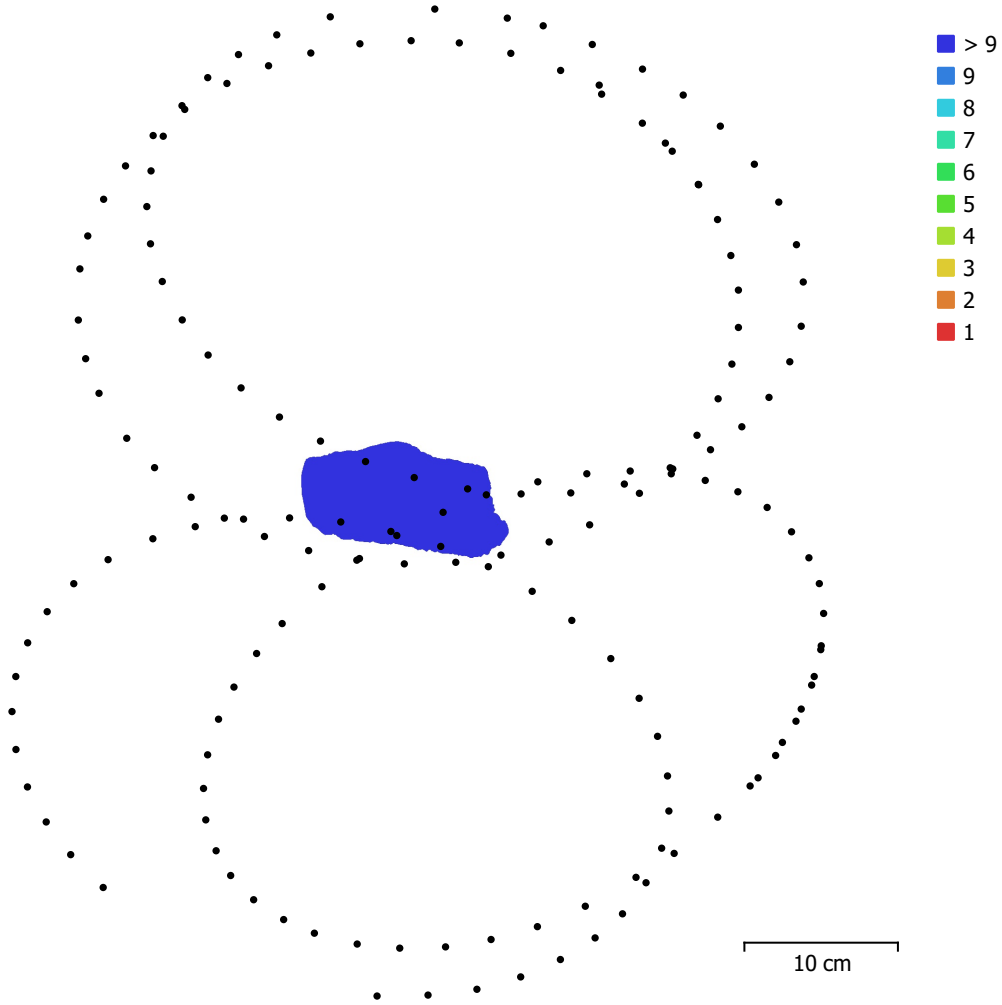

Fig. 1. Camera locations and image overlap.

Number of images:	165	Camera stations:	165
Flying altitude:	28.2 cm	Tie points:	54,674
Ground resolution:	0.0289 mm/pix	Projections:	243,037
Coverage area:	74.6 cm²	Reprojection error:	0.334 pix

Camera Model	Resolution	Focal Length	Pixel Size	Precalibrated
NEX-7, E 35mm F1.8 OS...	6000 x 4000	35 mm	4.04 x 4.04 µm	No

Table 1. Cameras.

Camera Calibration

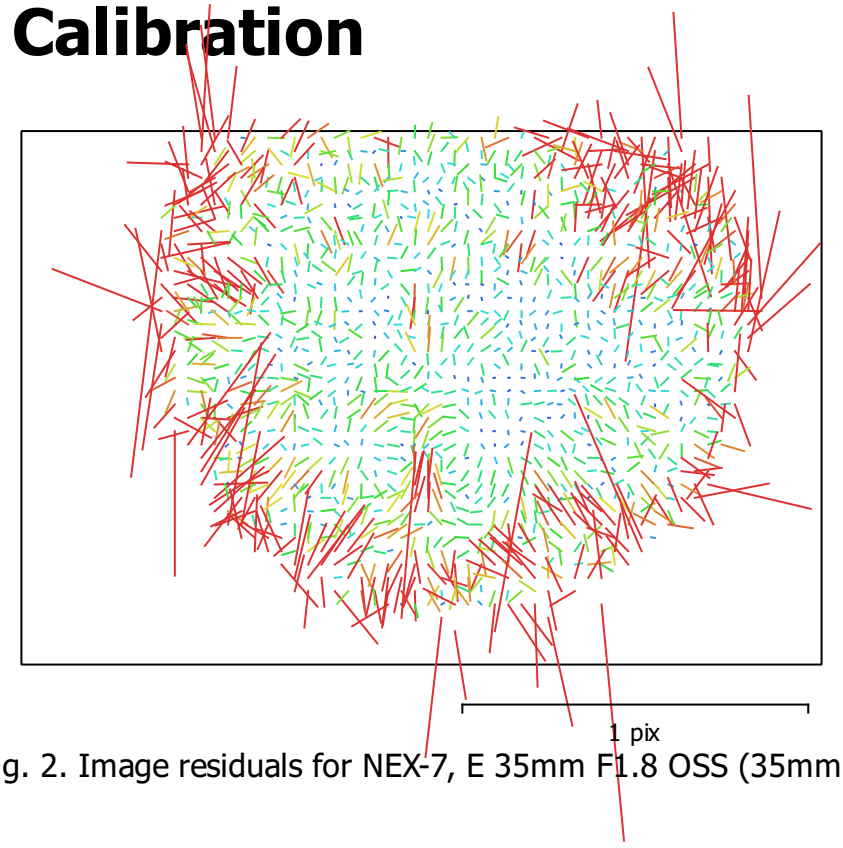

Fig. 2. Image residuals for NEX-7, E 35mm F1.8 OSS (35mm).

NEX-7, E 35mm F1.8 OSS (35mm)

165 images

Type	Resolution	Focal Length	Pixel Size
Frame	**6000 x 4000**	**35 mm**	**4.04 x 4.04 µm**

	Value	Error	F	Cx	Cy	K1	K2	K3	P1	P2
F	**9772.35**	0.93	1.00	-0.06	-0.22	-0.23	0.09	-0.10	0.06	-0.33
Cx	**-9.43975**	1.1		1.00	0.01	0.16	-0.14	0.13	0.94	0.14
Cy	**-27.8747**	0.67			1.00	-0.18	-0.00	0.02	0.10	0.11
K1	**0.0475383**	0.00078				1.00	-0.81	0.75	-0.01	0.46
K2	**-0.137515**	0.021					1.00	-0.97	-0.14	-0.02
K3	**-1.05782**	0.21						1.00	0.12	0.05
P1	**0.00140194**	4.3e-05							1.00	-0.13
P2	**0.00110019**	3.6e-05								1.00

Table 2. Calibration coefficients and correlation matrix.

Scale Bars

Label	Distance (m)	Error (m)
target 152_target 153	0.0500462	4.62156e-05
target 154_target 155	0.0499802	-1.9752e-05
target 156_target 157	0.0499409	-5.90828e-05
target 158_target 159	0.0500325	3.24786e-05
Total		**4.20466e-05**

Table 3. Control scale bars.

Digital Elevation Model

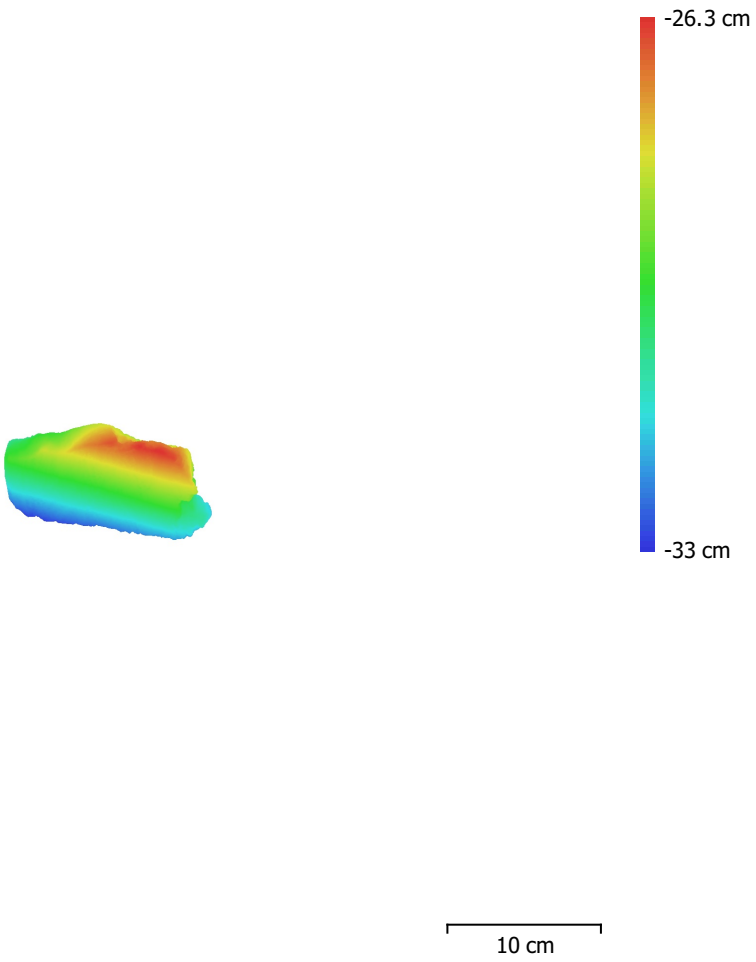

Fig. 3. Reconstructed digital elevation model.

Resolution:	unknown
Point density:	unknown

Processing Parameters

General	
Cameras	165
Aligned cameras	165
Markers	8
Scale bars	4
Coordinate system	Local Coordinates (m)
Rotation angles	Yaw, Pitch, Roll
Tie Points	
Points	54,674 of 330,959
RMS reprojection error	0.121736 (0.33424 pix)
Max reprojection error	0.407312 (1.79152 pix)
Mean key point size	2.67277 pix
Point colors	3 bands, uint8
Key points	No
Average tie point multiplicity	4.10099
Alignment parameters	
Accuracy	High
Generic preselection	No
Reference preselection	No
Key point limit	60,000
Key point limit per Mpx	1,000
Tie point limit	0
Exclude stationary tie points	Yes
Guided image matching	No
Adaptive camera model fitting	No
Matching time	3 hours 20 minutes
Matching memory usage	2.08 GB
Alignment time	3 minutes 6 seconds
Alignment memory usage	196.64 MB
Optimization parameters	
Parameters	f, cx, cy, k1-k3, p1, p2
Adaptive camera model fitting	No
Optimization time	2 seconds
Date created	2022:12:16 16:46:04
Software version	1.7.5.13229
File size	22.93 MB
Depth Maps	
Count	164
Depth maps generation parameters	
Quality	High
Filtering mode	Mild
Max neighbors	40
Processing time	1 hours 15 minutes
Memory usage	6.66 GB
Date created	2022:12:16 18:23:26
Software version	1.7.5.13229
File size	487.31 MB
Point Cloud	
Points	7,371,440
Point attributes	

Position	
Color	3 bands, uint8
Normal	
Confidence	
Point classes	
Created (never classified)	7,371,440
Depth maps generation parameters	
Quality	High
Filtering mode	Mild
Max neighbors	40
Processing time	1 hours 15 minutes
Memory usage	6.66 GB
Point cloud generation parameters	
Processing time	1 hours 27 minutes
Memory usage	10.99 GB
Date created	2022:12:16 19:51:07
Software version	1.7.5.13229
File size	148.36 MB
Model	
Faces	100,000
Vertices	50,002
Vertex colors	3 bands, uint8
Texture	16,384 x 16,384, 4 bands, uint8
Depth maps generation parameters	
Quality	High
Filtering mode	Mild
Max neighbors	40
Processing time	1 hours 15 minutes
Memory usage	6.66 GB
Reconstruction parameters	
Surface type	Arbitrary
Source data	Point cloud
Interpolation	Enabled
Strict volumetric masks	No
Processing time	4 minutes 57 seconds
Memory usage	3.80 GB
Texturing parameters	
Mapping mode	Generic
Blending mode	Mosaic
Texture size	16,384
Enable hole filling	Yes
Enable ghosting filter	Yes
UV mapping time	23 seconds
UV mapping memory usage	425.37 MB
Blending time	19 minutes 24 seconds
Blending memory usage	19.04 GB
Date created	2022:12:17 12:35:33
Software version	1.7.5.13229
File size	180.41 MB
System	
Software name	Agisoft Metashape Professional
Software version	2.0.0 build 15597
OS	Windows 64 bit
RAM	63.90 GB
CPU	Intel(R) Core(TM) i7-7700 CPU @ 3.60GHz
GPU(s)	Quadro M4000

ColSfM3-ARO18-02

Processing Report
18 May 2023

Survey Data

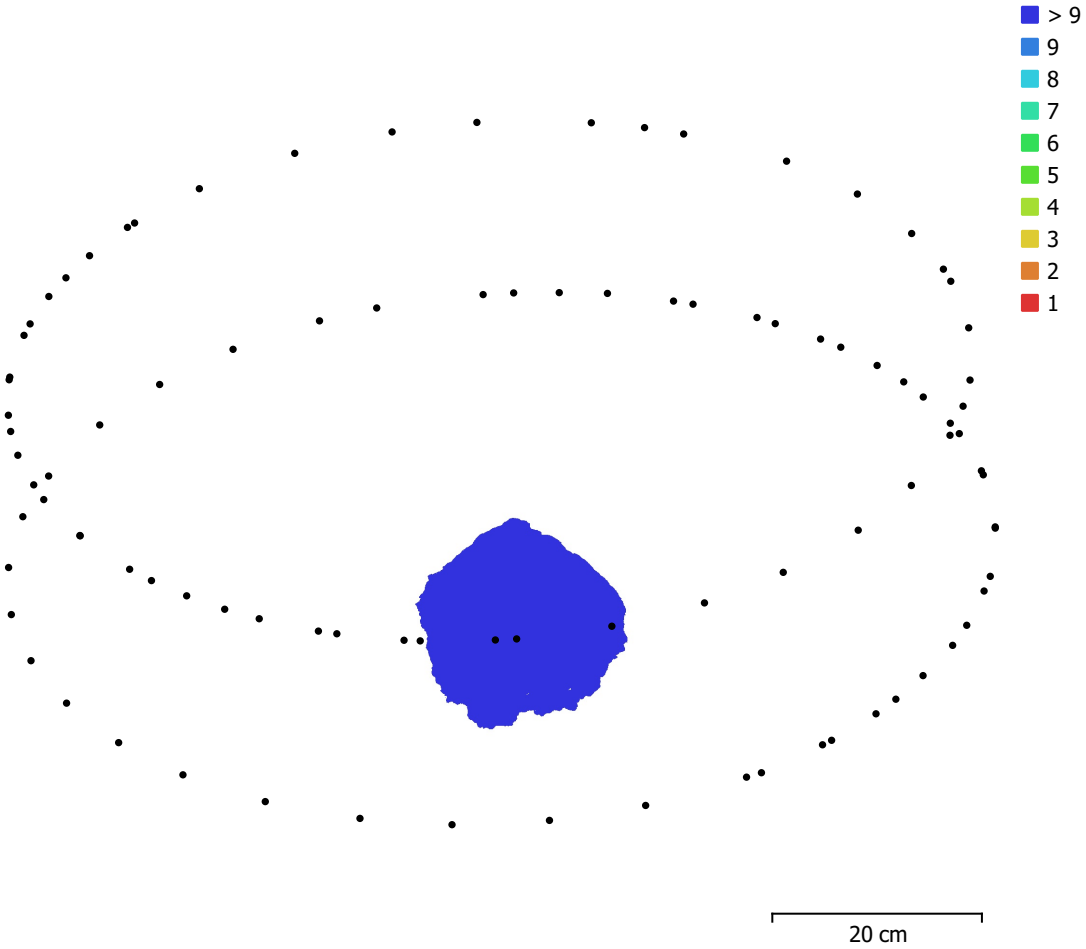

Fig. 1. Camera locations and image overlap.

Number of images:	97	Camera stations:	96
Flying altitude:	43.3 cm	Tie points:	61,140
Ground resolution:	0.0455 mm/pix	Projections:	236,418
Coverage area:	279 cm²	Reprojection error:	0.287 pix

Camera Model	Resolution	Focal Length	Pixel Size	Precalibrated
NEX-7, E 35mm F1.8 OS...	6000 x 4000	35 mm	4.04 x 4.04 µm	No

Table 1. Cameras.

Camera Calibration

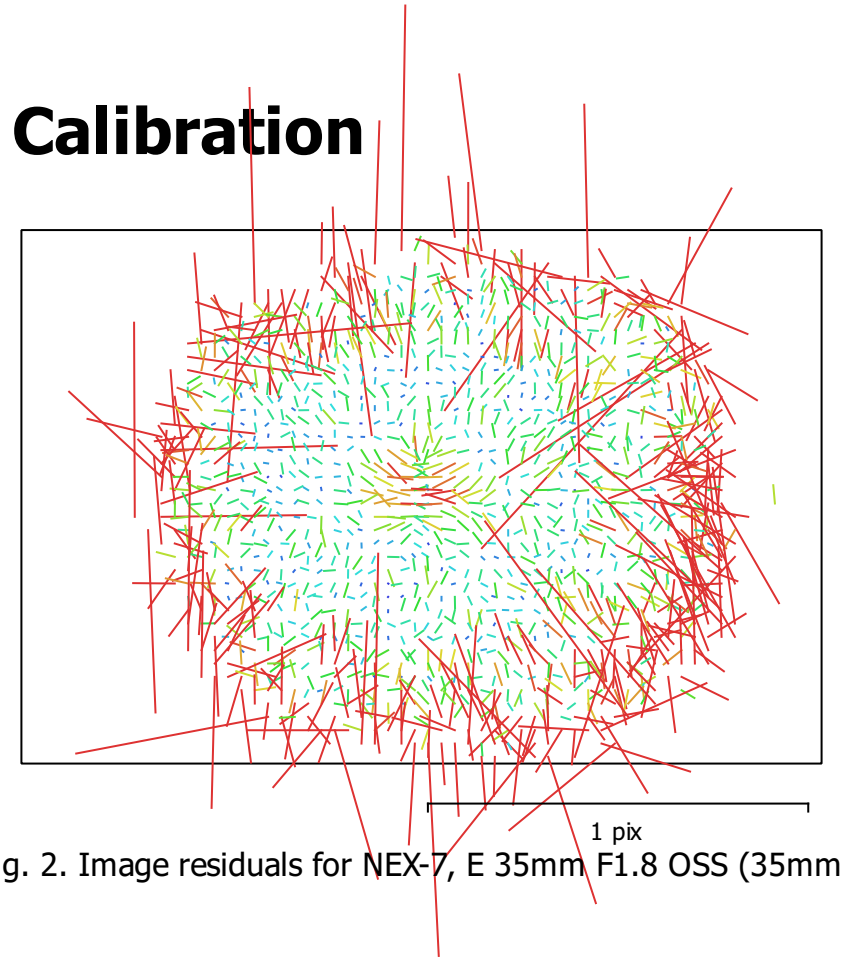

Fig. 2. Image residuals for NEX-7, E 35mm F1.8 OSS (35mm).

NEX-7, E 35mm F1.8 OSS (35mm)

97 images

Type	Resolution	Focal Length	Pixel Size
Frame	**6000 x 4000**	**35 mm**	**4.04 x 4.04 µm**

	Value	Error	F	Cx	Cy	K1	K2	K3	P1	P2
F	**9518.77**	1.7	1.00	-0.11	-0.57	-0.43	-0.03	0.01	-0.01	-0.31
Cx	**-17.8867**	1.4		1.00	0.02	0.05	0.07	-0.12	0.97	0.05
Cy	**-167.271**	2.5			1.00	0.06	0.05	-0.00	-0.05	0.78
K1	**0.00964277**	0.00079				1.00	-0.81	0.72	-0.00	0.06
K2	**0.810485**	0.028					1.00	-0.96	0.05	0.02
K3	**-10.5078**	0.32						1.00	-0.11	0.00
P1	**0.000107326**	8e-05							1.00	-0.03
P2	**5.80442e-05**	8.5e-05								1.00

Table 2. Calibration coefficients and correlation matrix.

Scale Bars

Label	Distance (m)	Error (m)
point 1_point 2	0.0940316	3.15686e-05
point 2_point 3	0.134406	-0.000594499
point 4_point 5	0.105727	0.000727253
Total		**0.000542624**

Table 3. Control scale bars.

Digital Elevation Model

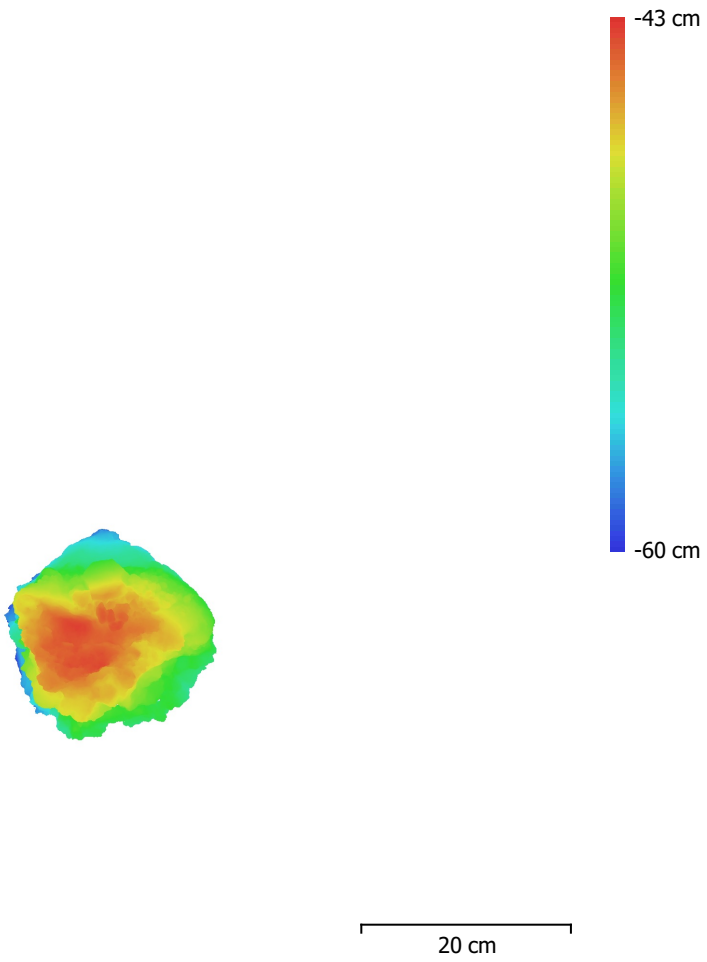

Fig. 3. Reconstructed digital elevation model.

Resolution:	unknown
Point density:	unknown

Processing Parameters

General	
Cameras	97
Aligned cameras	96
Markers	5
Scale bars	3
Coordinate system	Local Coordinates (m)
Rotation angles	Yaw, Pitch, Roll
Tie Points	
Points	61,140 of 409,461
RMS reprojection error	0.122815 (0.286662 pix)
Max reprojection error	0.339792 (1.17151 pix)
Mean key point size	2.30569 pix
Point colors	3 bands, uint8
Key points	No
Average tie point multiplicity	3.20089
Alignment parameters	
Accuracy	High
Generic preselection	Yes
Reference preselection	No
Key point limit	60,000
Key point limit per Mpx	1,000
Tie point limit	0
Filter points by mask	Yes
Mask tie points	No
Exclude stationary tie points	Yes
Guided image matching	No
Adaptive camera model fitting	No
Matching time	4 minutes 34 seconds
Matching memory usage	1.11 GB
Alignment time	2 minutes 3 seconds
Alignment memory usage	567.46 MB
Optimization parameters	
Parameters	f, cx, cy, k1-k3, p1, p2
Adaptive camera model fitting	No
Optimization time	2 seconds
Date created	2023:05:15 16:04:13
Software version	2.0.0.15597
File size	22.58 MB
Depth Maps	
Count	96
Depth maps generation parameters	
Quality	High
Filtering mode	Mild
Max neighbors	16
Processing time	1 hours 0 minutes
Memory usage	4.48 GB
Date created	2023:05:18 15:33:57
Software version	2.0.0.15597
File size	419.42 MB
Point Cloud	

Points	17,139,046
Point attributes	
Position	
Color	3 bands, uint8
Normal	
Confidence	
Point classes	
Created (never classified)	17,139,046
Depth maps generation parameters	
Quality	High
Filtering mode	Mild
Max neighbors	16
Processing time	1 hours 0 minutes
Memory usage	4.48 GB
Point cloud generation parameters	
Processing time	32 minutes 32 seconds
Memory usage	8.05 GB
Date created	2023:05:18 16:06:30
Software version	2.0.0.15597
File size	310.92 MB
Model	
Faces	10,043,564
Vertices	5,023,449
Vertex colors	3 bands, uint8
Depth maps generation parameters	
Quality	High
Filtering mode	Mild
Max neighbors	16
Processing time	1 hours 0 minutes
Memory usage	4.48 GB
Point cloud generation parameters	
Processing time	32 minutes 32 seconds
Memory usage	8.05 GB
Reconstruction parameters	
Surface type	Arbitrary
Source data	Point cloud
Interpolation	Enabled
Strict volumetric masks	No
Processing time	6 minutes 14 seconds
Memory usage	4.02 GB
Date created	2023:05:18 16:37:02
Software version	2.0.0.15597
File size	229.90 MB
System	
Software name	Agisoft Metashape Professional
Software version	2.0.0 build 15597
OS	Windows 64 bit
RAM	63.90 GB
CPU	Intel(R) Core(TM) i7-7700 CPU @ 3.60GHz
GPU(s)	Quadro M4000

8 References

Balco, G., Stone, J. O., Lifton, N. A. and Dunai, T. J.: A complete and easily accessible means of calculating surface exposure ages or erosion rates from ^{10}Be and ^{26}Al measurements, Quat. Geochronol., 3(3), 174–195, doi:10.1016/j.quageo.2007.12.001, 2008.

Leménager, M., Burkiewicz, J., Schoen, D. J. and Joly, S.: Studying flowers in 3D using photogrammetry, New Phytol., 237(5), 1922–1933, doi:10.1111/nph.18553, 2023.

Lifton, N., Sato, T. and Dunai, T. J.: Scaling in situ cosmogenic nuclide production rates using analytical approximations to atmospheric cosmic-ray fluxes, Earth Planet. Sci. Lett., 386, 149–160, doi:10.1016/j.epsl.2013.10.052, 2014.

Luhmann, T.: Close range photogrammetry for industrial applications, J. Photogramm. Remote Sens., 65(6), 558–569, doi:10.1016/j.isprsjprs.2010.06.003, 2010.

Mohren, J., Binnie, S. A., Rink, G. M., Knödgen, K., Miranda, C., Tilly, N. and Dunai, T. J.: A photogrammetry-based approach for soil bulk density measurements with an emphasis on applications to cosmogenic nuclide analysis, Earth Surf. Dyn., 8(4), 995–1020, doi:10.5194/esurf-8-995-2020, 2020b.

Over, J.-S. R., Ritchie, A. C., Kranenburg, C. J., Brown, J. A., Buscombe, D. D., Noble, T., Sherwood, C. R., Warrick, J. A. and Wernette, P. A.: Processing coastal imagery with Agisoft Metashape Professional Edition, version 1.6—Structure from Motion Workflow Documentation, Open-File Report, doi:10.3133/ofr20211039, 2021.

Vermeesch, P., Balco, G., Blard, P.-H., Dunai, T. J., Kober, F., Niedermann, S., Shuster, D. L., Strasky, S., Stuart, F. M., Wieler, R. and Zimmermann, L.: Interlaboratory comparison of cosmogenic ^{21}Ne in Quartz, Quat. Geochronol., 26, 20–28, doi:10.1016/j.quageo.2012.11.009, 2015.